JOURNAL OF GEOPHYSICAL RESEARCH, VOL. 106, NO. D16, PAGES 18,275–18,286, AUGUST 27, 2001

# Sahara mineral dust measurements from TOMS: Comparison to surface observations over the Middle East for the extreme dust storm, March 14-17, 1998

P. Alpert and E. Ganor
Department of Geophysics and Planetary Sciences, Tel Aviv University, Israel

**Abstract.** A comparison of the TOMS aerosol index (AI) with both measurements of dust concentrations and synoptic data over the Middle East for the extremely heavy dust storm of March 14-17, 1998, is performed. Time series over Algeria, Libya, and Israel yield the following findings: The peak values in both surface concentrations and TOMS data suggest that AI values of 2.5 and 1.2 correspond to surface mean daily concentrations of 1900 and 1000 $\mu g/m^3$ respectively. Surface concentrations and TOMS maps show that AI values of 3.0 correspond to about 4000 $\mu g/m^3$. TOMS AI maximum values were found to increase from Algeria to Israel moving along with the center of the dust plume from 0.9 to 2.1 and 2.5 AI values. This seems to be in contradiction with the fact that the plume moves farther away from the major mineral dust sources over the Sahara and may be caused by either an increased vertical extension of the plume, hence increasing the TOMS AI, or due to convergence of the dust plume over the eastern Mediterranean. The size distribution, morphological, and mineralogical composition of the dust analyzed in this study, as well as other aerosol parameters, are essential for improving the remote sensing methods such as the TOMS AI algorithms. Of course, surface measurements alone do not allow the refinement of the TOMS retrievals; vertical profile dust measurements as well as other physical and optical aerosol parameters are necessary.

## 1. Introduction

Dust has a major influence on rainfall, human welfare, water, and soil composition, as shown by many studies [e.g., *Pye*, 1987, *Schulz et al.*, 1990], and, in particular, over Israel and the Middle East [*Levin et al.*, 1996; *Ganor and Foner*, 1996]. The various potential impacts over the Mediterranean region are reviewed by *Guerzoni and Chester*, [1996]. In addition, in the global sense, dust covers large regions over both land and oceans. Persistent dust transport over the Atlantic Ocean has been measured in Barbados and Florida [*Prospero and Nees*, 1986]. Dust dominates the NOAA images of aerosol over the ocean [*Husar et al.*, 1997]. About 50% of the dust is associated with anthropogenic sources [*Tegen et al.*, 1996]. The crucial role of mineral dust and other aerosols in climate has been recently emphasized in studies of the potential greenhouse gas warming effects [e.g., *IPCC*, 1996]. Along with the increased awareness to the importance of mineral dust and other aerosols in climate [e.g., *Alpert et al.*, 1998], enhanced efforts were done to better monitor the atmospheric aerosols on a more regular basis. Recent successes using remote sensing over oceans are striking [*Husar et al.*, 1997; *Tanre et al.*, 1997]. Preliminary, dust climatologies have been performed, as for instance the 5 year study by *Jankoviak and Tanre* [1992] over the east Atlantic. Such climatologies along with atmospheric dynamical data also allow studies of the relationships between dust and synoptic systems as the North Atlantic oscillation [*Moulin et al.*, 1997]. For global remote dust detection, the AVHRR observations, for instance, are mostly limited to over water because of the requirement for low, non-variable surface reflectivity. A new technique for detecting UV–absorbing aerosols in the atmosphere is based on the spectral contrast between two of the Total Ozone Mapping Spectrometer (TOMS) channels, i.e., a ratio of 340-380 nm radiance, available from the NIMBUS-7 satellite from November 1978 to May 1993. A new TOMS instrument on the NASA Earth probe satellite was launched July 2, 1996, [*Herman et al.*, 1997].

The UV spectral contrast method does not suffer from the limitation of visible-wavelength techniques, since the UV surface reflectivity is low and nearly constant over both land and water. Hence the global daily coverage for the UV-absorbing aerosols available



Paper number 2000JD900366.
0148-0227/01/2000JD900366$09.00

through this technique are a major experimental component of the analysis in the present work with a focus over an extremely severe dust storm event over the Middle East.

Recently, *Hsu et al.* [1999], have compared TOMS aerosol index (AI) with AERONET optical thickness at several stations over the globe and derived relationships based on the correlations they found. In the present study we focus on the regional evolution of the extremely heavy dust storm of March 14-17, 1998. This, by comparison of the mineral dust estimation from TOMS data with both the surface dust loading and the synoptic observations over the Middle East. It is of our interest to investigate the relationship between the two distinct dust measures, despite the fact that they do not coincide in space. In fact, they complement each other because the TOMS AI provides a vertically integrated measure of dust which mostly excludes the near-surface dust, as discussed next.

## 2. Methodology

### 2.1. Detection of Aerosols by TOMS Instrument

*Herman et al.* [1997] proposed a new technique for detecting UV–absorbing aerosols in the atmosphere based on the spectral contrast of the 340 and the 380 nm radiances. These are two of the Total Ozone Mapping Spectrometer (TOMS) channels available from the NIMBUS-7 satellite. The UV spectral contrast method does not suffer from the limitation of visible-wavelength techniques, since the UV surface reflectivity is low and nearly constant over both land and water. The coverage for the UV-absorbing aerosols available through this technique serve as a central experimental component in the present study. There is some cloud contamination that is unavoidable in the TOMS AI signal. The data are filtered for clouds by only including pixels for which the scene reflectivity is no more than 10% above the known surface reflectivity. Therefore in the $100 \times 100 km^2$, there can be a small amount of sub pixel contamination. Saharan dust particles decrease the reflectivity below the background by a few percent, while small-particle dust can increase the reflectivity by 2 to 3%. Smoke or non-UV-absorbing aerosols (e.g., sulfate) will increase the reflectivity by 3 to 5%,[*Alpert et al.*, 2000]. Another limitation of the TOMS AI is its inability to fully detect the aerosols within the 1-2 km above the surface [*Herman et al.*, 1997].

### 2.2. Surface Sampling of Dust

Dust particles were collected isokinetic near the ground, on policarbonate membrane 0.4 and 0.8 $\mu$m pore size for 20 to 40 min. For individual particles the chemical, morphological, and size distribution were analyzed. In addition, dust was collected on Watman membrane filters 47 mm diameter, 0.45 pore size for 4 hours for chemical and mineralogical analysis. Automated particulate mass concentrations were monitored by TEOM series 1400A. The instrument incorporates a true micro-weighing technology developed by Rupprecht and Patashnick Co. Inc. In Tel Aviv stations we measured mass concentration of PM-10. The size distribution and chemical composition of selected specimens were investigated by X-ray analysis using a JEOL 6300 scanning electron microscope (SEM) equipped with a Link -ISIS 10,000 energy dispersive system (EDS). The spectrometer of the EDS system separate the elements according to energy rather than wavelength. Quantitative analysis was performed by ZAF 4 program, and 431 particles were analyzed for their elements and size distribution. In addition, a petrographic microscope was used to identify minerals. Mineralogical analyses were carried out by X-ray diffraction using a Phillips PW 1820 diffraction and Cu Ka radiation, as described by *Ganor* [1991]. Chemical composition of suspended and settling dust particles were analyzed by inductively coupled plasma automatic emission spectrometry (ICP), as described by *Ganor et al.* [1991].

## 3. Synoptic Conditions

Figures 1a-1d show the surface sea level pressure charts for March 14-17, 1998. On March 14, 1998, the Sharav cyclone is located over central North Africa south of the Sirte Gulf (28°N, 13°E) (Figure 1a), with a central sea level pressure ( SLP) of 1002 hPa. Twenty-four hours later, the cyclone moved quickly northeastward to the east Mediterranean (EM) coast at the Libya-Egypt border (32°N, 25°E), while deepening to 990 hPa. This corresponds to a high speed of about 15 $ms^{-1}$ which was reported earlier as typical for Sharav cyclones during spring. This speed is significantly higher than for the cold winter cyclones over the Mediterranean [*Alpert and Ziv*, 1989]. On the following day, the cyclone progressed quickly in the same northeastward direction reaching the north-eastern corner of the Mediterranean. At the same time, an extremely heavy

**Figure 1.(a–d)** Surface sea–level–pressure charts for for 1200 UTC March, 14-17, 1998, over the Mediterranean region (15°N-60°N, 10°W-60°E) (in panels a-d, respectively). On 14, March 1998, the Sharav cyclone is located over central North Africa south of the Sirte Gulf (28° N, 13° E) (Figure 1a) with a central sea level pressure ( SLP) of 1002 hPa. The sea-level-pressure contour interval is 2 hPa. Data are from the European Center of Medium-Range Weather Forecastings (ECMWF) analysis.

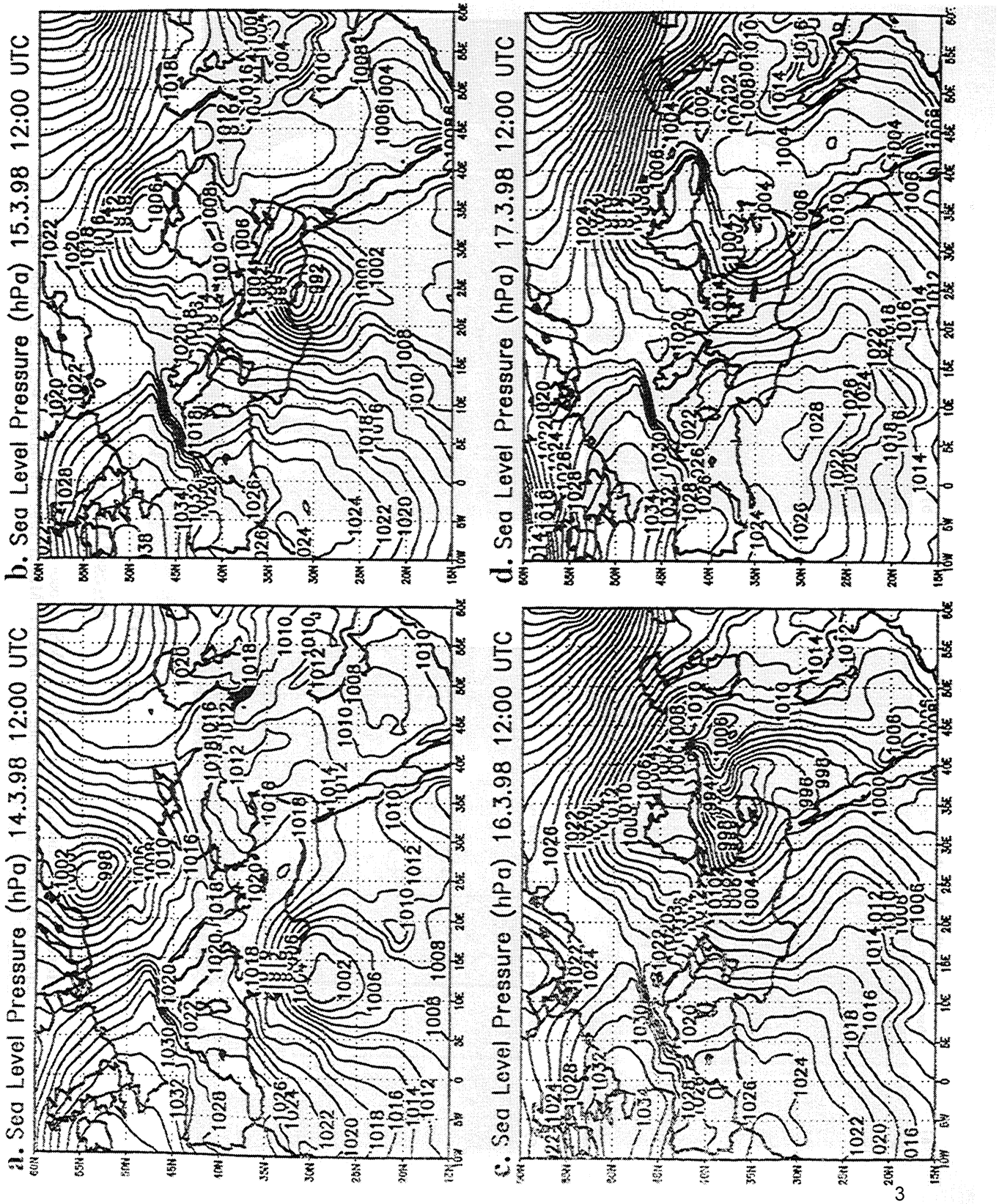
a. Sea Level Pressure (hPa) 14.3.98 12:00 UTC
b. Sea Level Pressure (hPa) 15.3.98 12:00 UTC
c. Sea Level Pressure (hPa) 16.3.98 12:00 UTC
d. Sea Level Pressure (hPa) 17.3.98 12:00 UTC

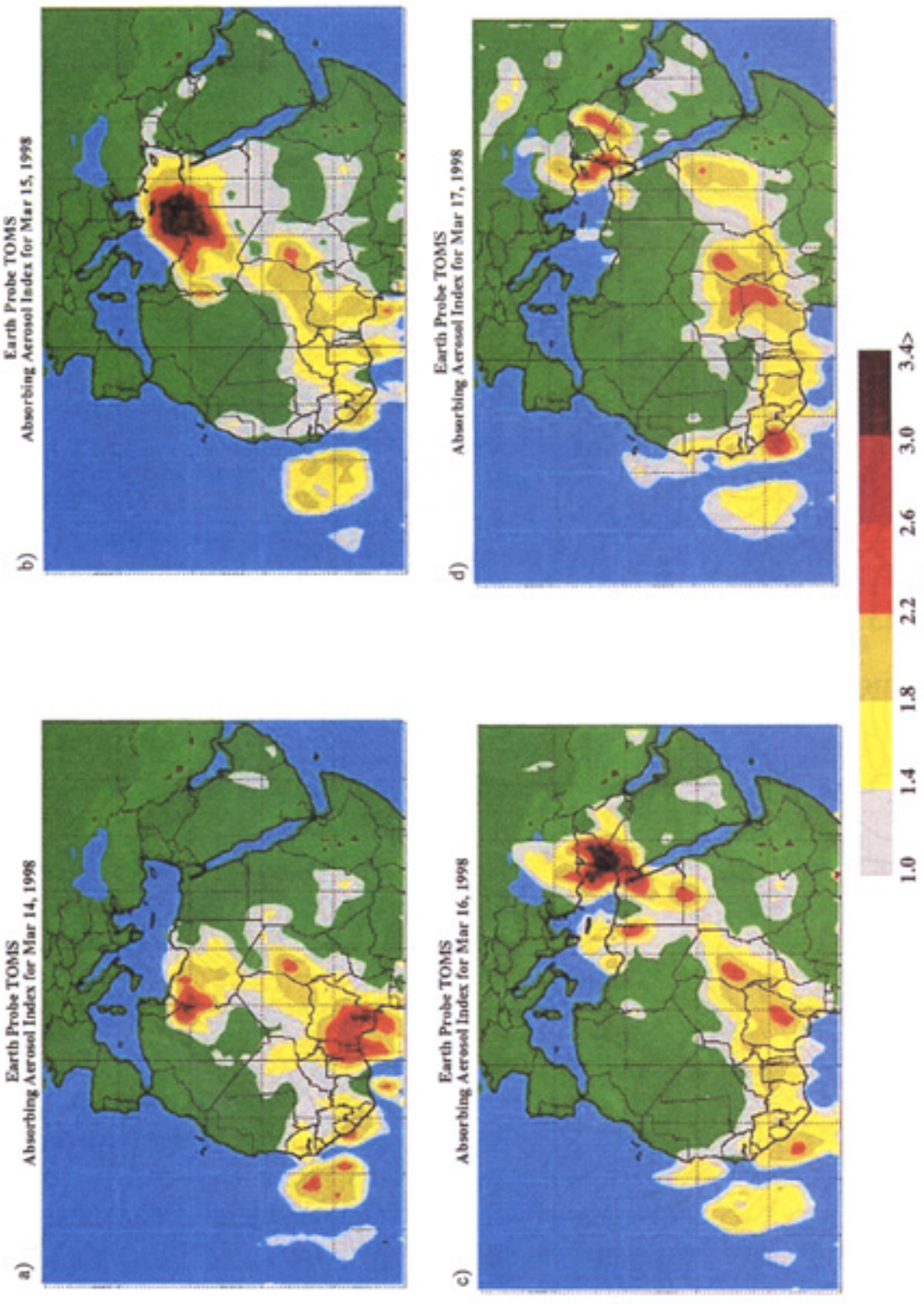


**Plate 1. (a-d)** distributions of the TOMS aerosol index (AI) over North Africa, Mediterranean and the Middle East for the period of 14-17, March 1998 (in panels a-d). The color bar at the bottom indicates the AI values.

dust plume covered the EM and Israel, the focus of the present study.

The time series for SLP in Tel Aviv indicates a minimum of 990 hPa at 2330 LT, March 15 (not shown). The surface pressure dropped from 1010 hPa at 0700 (to 990 hPa). This is a pressure drop larger than 1 Bergeron when adjusted to Tel Aviv latitude of 32°. Such a minimum of SLP is extremely rare over the EM.

Figures 2a and 2b show the NOAA satellite pictures in which the dust plume transport over the EM from March 15, 1436 LT to March 16, 1436 LT is clearly seen. In Figure 2a the dust is located over north Egypt and the southeastern part of the Mediterranean, while Sinai and Israel are still clear. Twenty-four hours later (Figure 2b), the dust plume covers the EM, including Sinai, Israel, Jordan, and extending north-northeastward to Syria and east Turkey.

## 4. TOMS Data

Plates 1a-1d show the geographical distributions of the TOMS AI over North Africa, the Mediterranean, and the Middle East for the period of March 14-17, 1998. These are Sun-synchronous pictures at a near-noon (≈1100 LT) orbit of the Earth probe/TOMS launched July 2, 1996, [*Herman et al.*, 1997]. In contrast to the case study by *Herman et al.* [1997] in which the dust plume moved in the westward sector, a major Middle East dust plume moving eastward is noticed in Plates 1a-1d. In particular, it is interesting to note the fast dust plume longitudinal transport of about $12° - 14°$, as described by *Ganor* [1975] and *Alpert and Ziv* [1989]. This is about 20-25% faster compared to the speed of the surface cyclone (Figure 1a-1d) and will be discussed further (Figure 8). An-

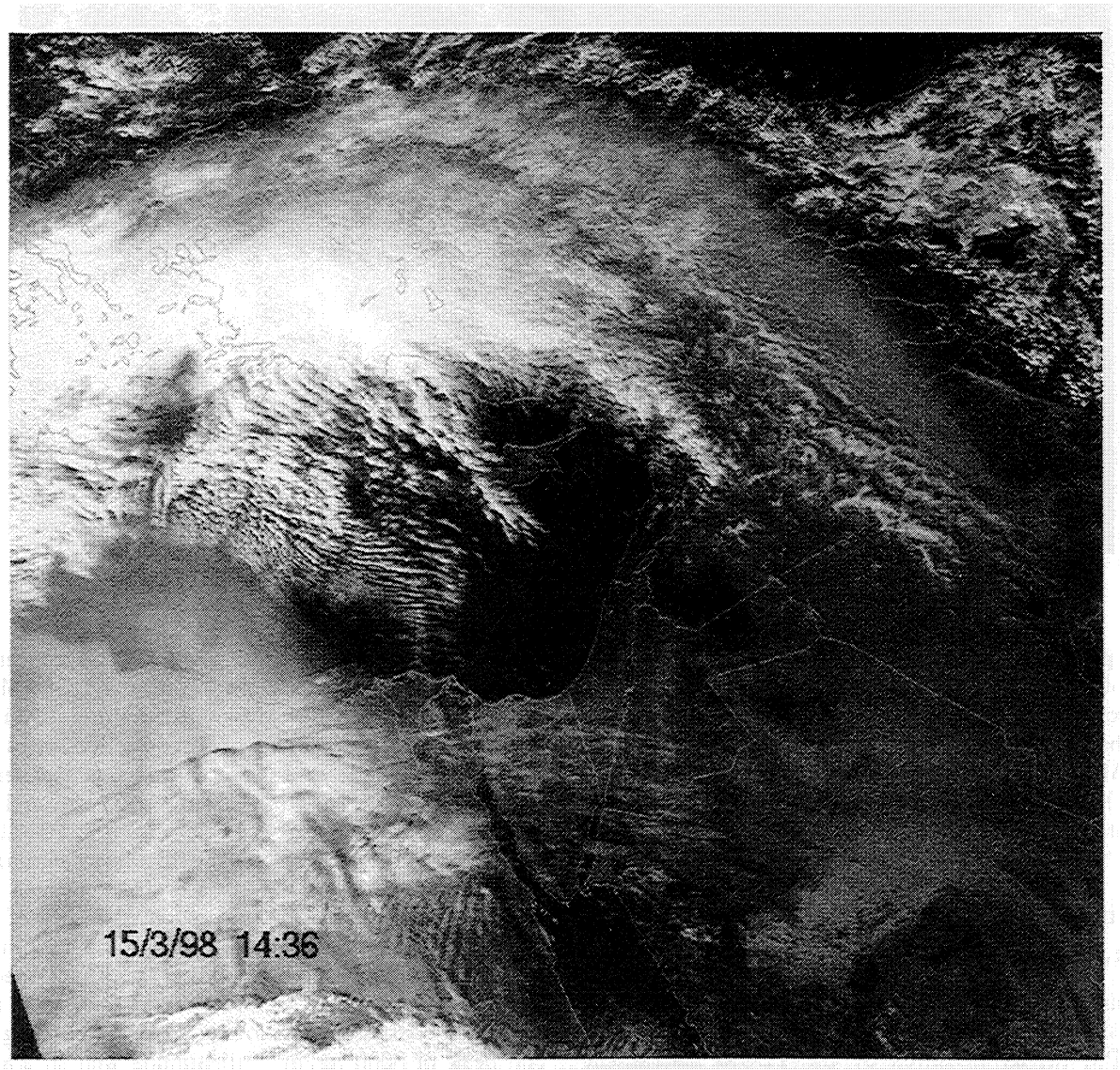


**Figure 2. (a,b)** NOAA satellite pictures with the dust plume over the Eastern Mediterranean for 1436 LT, 15 and 16, March 1998, respectively. In Fig. 2a the dust plume is located over north Egypt and the southeastern part of the Mediterranean, while Sinai and Israel are still clear. Twenty-four hours later (Figure 2b), the dust plume covers the EM, including Sinai, Israel, Jordan, and extending north-northeastward to Syria and east Turkey.

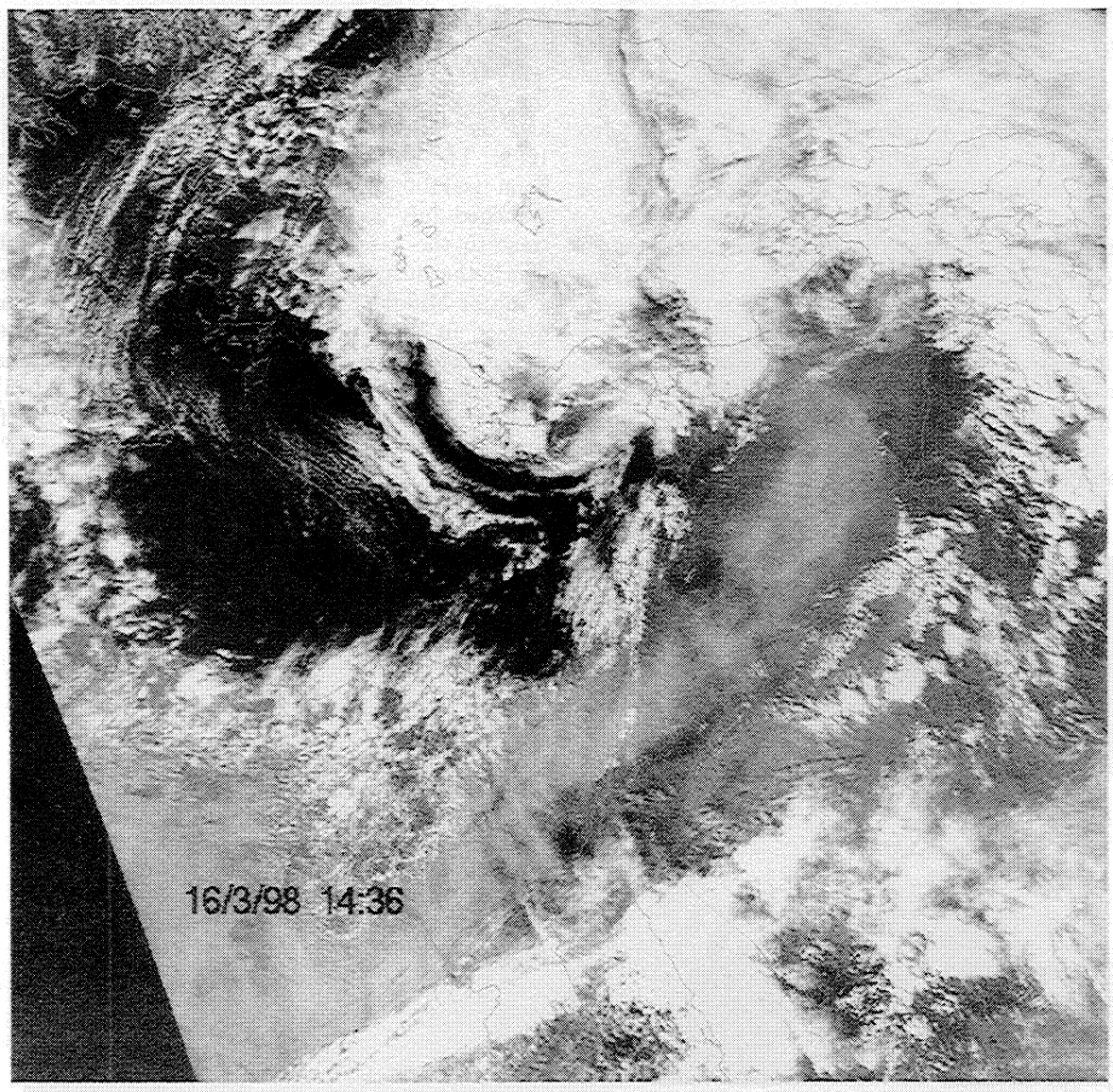


Figure 2. (continued)

other prominent feature is the dramatic increase of the dust plume both in the geographical area and in the dust concentrations as expressed by the AI in Plates 1a and 1b. On the third day (Plate 1c), the plume reaches the EM and covers the whole region including Israel in which local dust measurements have been taken and are presented in section 5.

## 5. Dust Data

### 5.1. Surface Dust Loading Measurements

Figures 3a-3b show time series of dust concentrations of particulate matter of less than 10 $\mu$m size in diameter (PM-10) as measured by the TEOM instrument located in north Tel Aviv. In Figure 3a the diurnal averages for the whole month of March are presented, showing a most pronounced peak on 16 March of 1900 $\mu g/m^3$ corresponding to the major event discussed in the present work, i.e., compare to the TOMS AI in Plate 1c. A secondary maximum of dust concentration is found 11 days later on 27, March 1998. March is indeed one of the most dusty months in Tel Aviv, as discussed by *Ganor* [1994]. Figure 3a illustrates that the background concentrations during nondust periods are of about 30-50 $\mu g/m^3$. A time zooming on 15-16, March is given in Figure 3b where 30 min PM-10 averages are presented around the 16 March climax. A very sharp increase of PM-10 is noticed between 0300 and 0700 LT reaching an unprecedented record of 8000 $\mu g/m^3$. Nearly all other aerosol-monitoring instruments in the region of Israel (six in number) malfunctioned because of the extremely high loading at this stage; most instruments stopped functioning at about 2000 $\mu g/m^3$. The peak of 8000 $\mu g/m^3$ corresponds well to another measurement of 9000 $\mu g/m^3$ by a beta sampler of Total Suspended Particles (TSP) located at another north Tel Aviv neighborhood (not shown). The rates of dust increase/decrease are of the same magnitude of about 35 $\mu g/m^3$/min yielding about 3-4 houres from the time

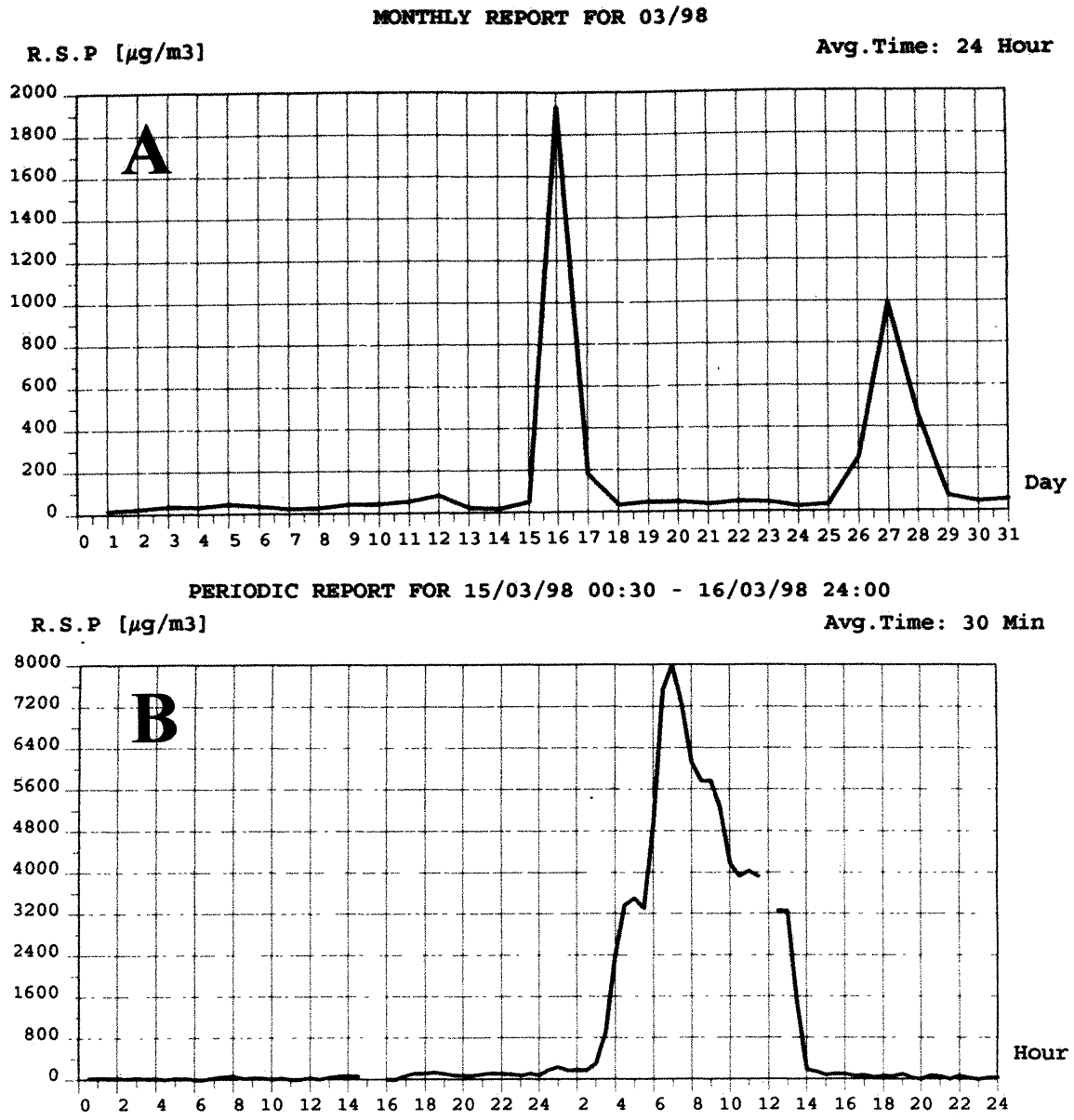


**Figure 3.(a-b)** Time series of dust concentrations of particulate matter (in $\mu g/m^3$) of less than 10 $\mu m$ size in diameter (PM-10) as measured by the TEOM instrument located in north Tel Aviv (Shikun Lamed, Electric Co. measurement). In Figure 3a, diurnal averages for the whole month of March are presented, while Figure 3b presents 30 min average for the 15-16, March 1998.

of near background value of 50 to the peak loading of 8000 $\mu g/m^3$. An exception to that is the higher rate of about 50 $\mu g/m^3$/min corresponding to the rainfall washout at the last stage of dust removal, for example, the steep slope of the PM-10 curve between 1300 and 1400 LT in Figure 3b. The total duration of this heavy dust event is therefore of about 13 hours beginning 3 hours past midnight to 1400 LT on 16, March 1998. It is interesting to note that the washout of the dust was associated with extremely cold air and even snow in Jerusalem. Snow in mid-March is rare, as discussed by *Alpert and Reisin* [1986] and it needs yet to be explored if there is any microphysical reason behind this late snow associated with ice nuclei of mineral dust.

### 5.2. Comparison of Dust Concentrations to TOMS AI

In this section we try comparing the Tel Aviv time series of the dust concentration from Figure 3b (PM-10, in brevity) and the TOMS AI of Plate 1c. The time extension of above 4000 $\mu g/m^3$ in the PM-10 graph is of about 6 hours, i.e., 0600-1200 LT, and is prior to the last stage of the fast rain washout. Now, the geographical extension of TOMS AI above the index of 3.0 in Plate 1c is of about 350 km and with a dust plume speed of 15 $ms^{-1}$ (as calculated in the preceding section) also yields a time span of about 6 hours. Hence the TOMS AI of 3.0 seems to roughly correspond to about 4000 $\mu g/m^3$

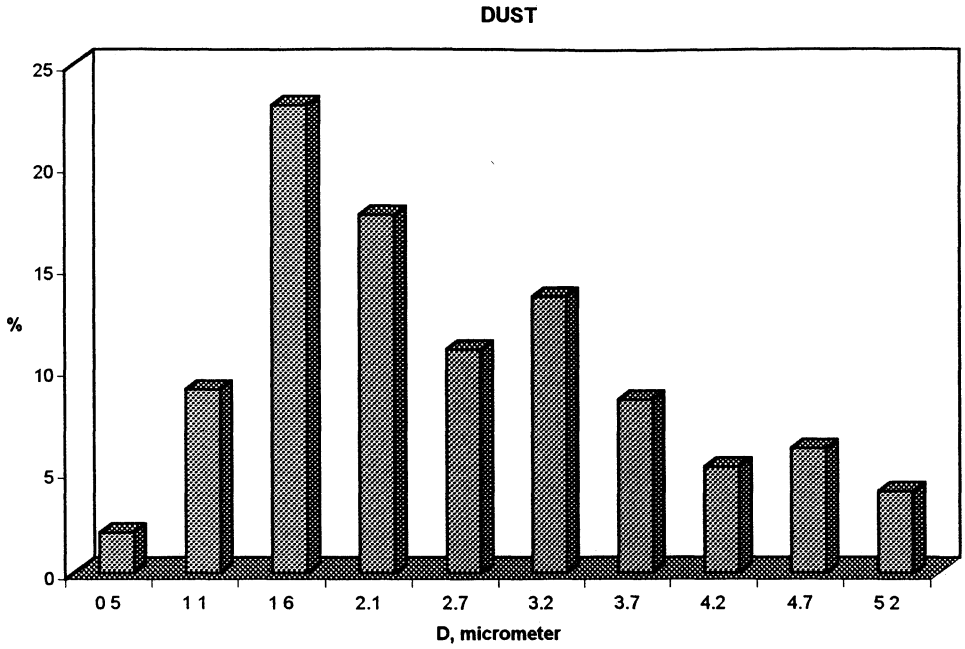


**Figure 4.** Size distribution (in percent) of suspended particles on 16, March 1998. This is based on the scanning electron microscope image analysis of 431 particles.

of the surface measurements. The depth of the heavy dust reported by pilots over Israel, Tel Aviv region, at about 1000-1200 LT was of about 6000 feet or about 2 km, which suggests that the TOMS AI of 3.0 for the upper layer (1-2 km) corresponded to the surface local concentration of about 4000 $\mu g/m^3$.

The total dust mass for a cylinder having the height of about 2 km and the diameter of 330 km (corresponding to the dust with AI>3.0, Plate 1c) and average concentration of 3500 $\mu g/m^3$ is about 600 $\times 10^9$ gr. This value is so exceptional over the Mediterranean that it fits peaks of monthly averaged suspended dust mass

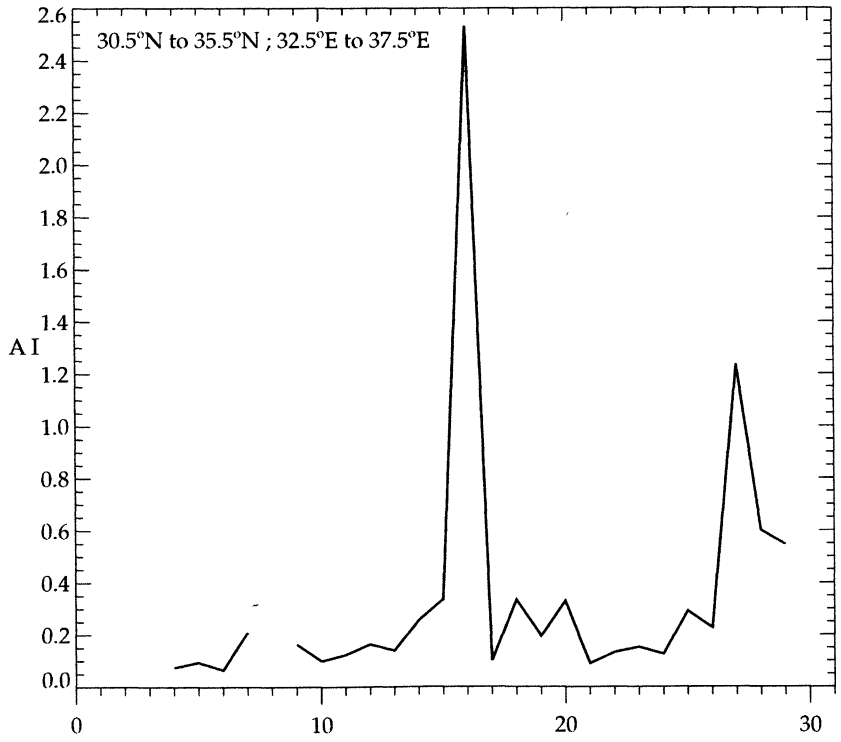


**Figure 5.** Time series of the dust TOMS AI over Tel Aviv region (30.5°-35.5°N, 32.5°-37.5°E) during March 1998.

over the Mediterranean, as reported by *Dulac et al.* [1996, Figure 4].

### 5.3. Size Distribution and Mineralogical Analysis

Figure 4 shows the size distribution of suspended particles on 16, March 1998, and the most frequent size is of about 1.6 $\mu$m diameter. The majority of the particles are in the range of 1-5 $\mu$m (90% of the 431 particles sampled). In particular, the following values were found: the most frequent size is 1.2-2.1 $\mu$m $\approx$ 40%; a secondary peak is at the size of 2.8-3.2 $\mu$m. This distribution shows a wide range of dust sizes typical for heavy dust storms. Mineralogical analysis carried out by X-ray diffraction (see section 2) yields that most of the nonclay minerals contain calcite (29%), quartz (29%), gypsum (5%), feldspar (8%), dolomite (26%), and clay minerals of illite, kaolinite and palygorskite.

## 6. Discussion

### 6.1. Comparison of TOMS AI and Surface Dust Concentration

Figure 5 shows the time series of the dust TOMS AI over Tel Aviv during March 1998. Two pronounced maxima are noticed, on 16 and 27 March with AI dust values of 2.5 and 1.2, respectively. The background value before the major event of 16 March is below 0.2 with two small peaks of 0.3 on 18 and 20 March.

Comparing this pattern to that shown by the surface-averaged dust concentration, also in Tel-Aviv, Figure 3a, reveals a similar pattern of the two major events. The surface background concentrations, however, are much smoother, with values less than 50 $\mu g/m^3$. One explanation for this apparent inconsistency in the background levels may be potential high-altitude dust layers which are captured by the TOMS but do not have any surface signature. Another important difference between the two graphs (figures 5 and 3a) is the fact that the surface concentrations are composed from daily averages (every 30 min), while the TOMS presents a single daily measurement before noon. This, for instance, could explain the relatively high surface concentration on 17 March which is not measured by the TOMS. In addition, the TOMS AI values are spatial averages over $5° \times 5°$ compared to a point measurement over Tel Aviv.

The peak values in both graphs suggest that AI values of 2.5 and 1.2 correspond to surface mean daily concentrations of 1900 and 1000 $\mu g/m^3$, respectively. In addition, the surface background concentrations of 50 $\mu g/m^3$ compare to about 0.1-0.2 AI value. In section 5b when analyzing the geographical extensions of the dust plume, a correspondence between AI of 3.0 and 4000 $\mu g/m^3$ concentration was deduced. These events suggest some relationship between the TOMS AI and the surface concentrations. Obviously, further evaluation of these results requires additional comparisons. It is interesting to note that *Hsu et al.* [1999] have shown that TOMS AI measurements are linearly proportional to the aerosol optical thickness (AOT) derived from surface Sun photometer instruments. However, both of these measurements, i.e., of aerosol optical thickness and of the TOMS AI are column-integrated measures in contrast to the surface measurements.

### 6.2. An In-Conjunction Tracking of the Synoptics, Dust Plume and TOMS AI

Figure 6 shows the time series of the Dust TOMS AI over Algeria, Libya and Israel (Tel Aviv), during 12-21, March 1998; the locations of the three points are shown in Figure 7. This graph zooms over 10 days of March (12-21 March) which was given earlier for Tel Aviv, (Figure 5). The three locations are on the route of the dust plume, as shown by the TOMS AI maps given in Plates 1a-1d. It is interesting to note that the TOMS AI maximum values increase from Algeria to Israel moving along with the center of the dust plume from 0.9 to 2.1 and 2.5 AI values. This seems to be in contradiction with the fact that the plume moves farther away from the major mineral dust sources over the Sahara, [*Alpert and Ganor*, 1993; *Guerzoni and Chester*, 1998]. A possible explanation is either an increased vertical extension of the plume, thus increasing the TOMS AI, or a convergence of the dust plume over the eastern Mediterranean.

Figure 7 shows the location of the TOMS AI dust plume relative to the cyclone's track on 14, 15 and 16, March 1998. The plume boundaries are based on Plates 1a-1c at the AI values of 2.2 and 3.0 (horizontal and vertical line shading) which represent the areas of high and very high TOMS-deduced dust-integrated concentrations. We wish to note that the position of

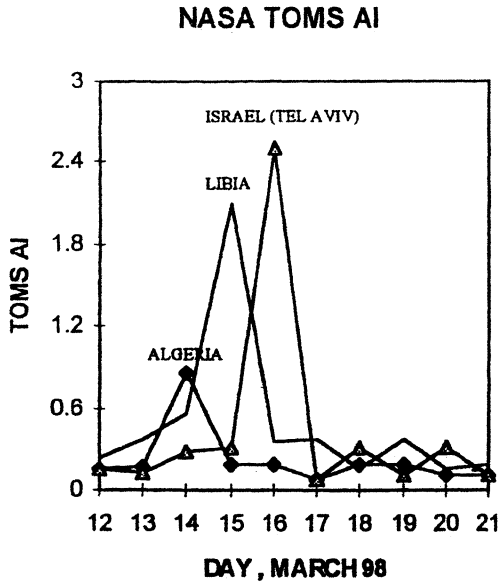


**Figure 6.** Time series of the dust TOMS AI over Algeria, Libya and Israel (Tel Aviv) regions, during 12-21, March 1998. Values are averaged over $5° \times 5°$, and the central points locations are shown in Figure 7 by three large circles.

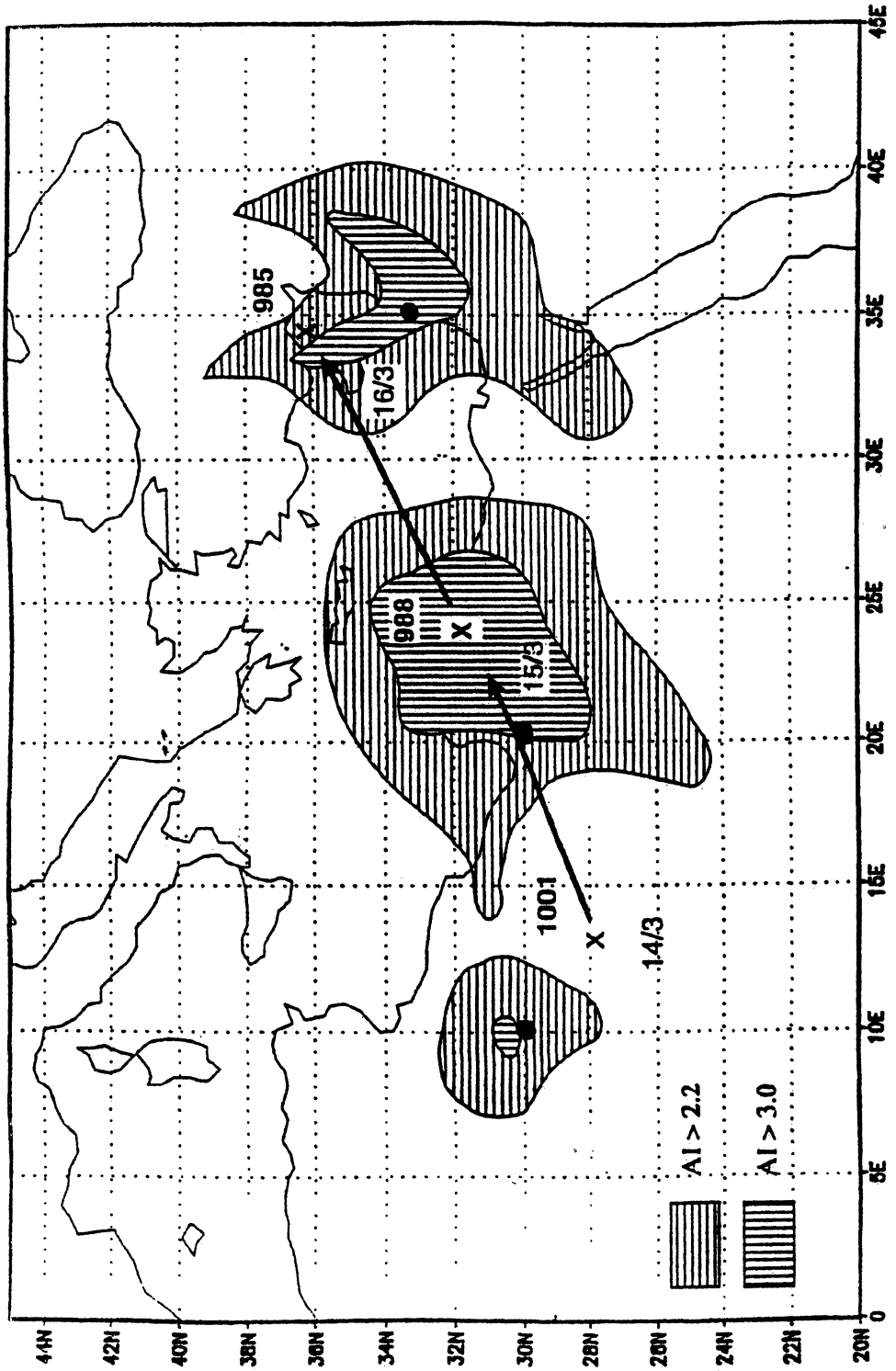


**Figure 7.** Location of the TOMS AI dust plume relative to the cyclone's track on 14, 15 and 16, March 1998. The plume boundaries are based on Plates 1a-1c at the AI values of 2.2 and 3.0 and are represented by the horizontal and vertical line shadings, respectively, see inset at the bottom left. The cross signs denote locations of the cyclone center based on the minimum sea level pressure whose value (in hPa) for each day is marked above the cross. The large circles are the points for the TOMS AI time series in Figure 6.

the central dust region changes considerably relative to the cyclone's center in the following manner. On 14 March the dust plume ( at about 30°N, 10°E) is located northwest to the cyclone center. Then, on 15 March it becomes colocated with the cyclone and 24 hours later, on 16 March the plume moves to the southeast of the cyclone's center. However, this transport may not reflect the realistic movement of the dust plume, since the TOMS AI pictures provide only an integrated measure and the significant vertical wind shear, which is common in a cyclone region, would be expected to disperse the plume according to the dominant winds in each layer.

Another interesting result mentioned earlier is the higher concentrations over the Tel Aviv region (Figure 6) compared to Algeria and Libya, which are closer to the sources of the dust storms. This may be explained by the deepening of the cyclone on its track to the EM as illustrated by the considerable drop in the cyclone's central pressure, i.e., from 1001 hPa in Algeria to 988 and 985 hPa over Libya and the EM, respectively.

## 7. Summary

In the present study we have performed a first comparison of the mineral dust estimation from TOMS data with the surface and synoptic observations over the Middle East for the extreme dust storm of 14-17, March 1998. Comparing the surface observations of the dust concentrations in Tel Aviv, Israel, and the TOMS AI geographic maps as well as time series over Algeria, Libya and Israel yields the following findings; The peak values in both surface concentrations and TOMS data suggest that AI values of 2.5 and 1.2 correspond to surface mean daily concentrations of 1900 and 1000 $\mu g/m^3$, respectively. When analyzing geographical extensions of the dust plume, a correspondence between AI of 3.0 and 4000 $\mu g/m^3$ concentration was deduced. Similar studies by tracking of the synoptics in conjunction with the dust plume concentration measurements and the TOMS AI will allow a better evaluation of the TOMS AI pictures. In general, the size distribution, morphological and mineralogical composition of the dust, as well as all other aerosol parameters are essential for improving the remote sensing methods such as the TOMS AI algorithms. Of course, surface measurements alone do not allow the refinement of the TOMS retrievals; vertical profile dust measurements as well as other physical and optical aerosol parameters are necessary.

**Acknowledgments.** The study was supported by the US-Israel Binational Science Foundation grant 97-00448. We wish to express our gratitude to S. Krichak and A. Beharad for help in drawing the maps. Thanks to J. Herman and D. Larko, NASA GSFC, for help with the TOMS graphs and maps. Thanks to M. Dvorachek for assistance in the electron microscope and Bat-Sheva Cohen, Geological Survey of Israel, for drawing Figure 7. Thanks to C. Shafir for final preparation of manuscript.

## References

Alpert, P., and Ganor, E., A jet-stream associated heavy dust storm in the western Mediterranean, *J. Geophys. Res., 98*, 7339-7349, 1993.

Alpert P. and T. Reisin, An early winter polar airmass penetration to the eastern Mediterranean, *Mon. Weather Rev., 114*, 1411-1418, 1986.

Alpert, P. and B. Ziv, The Sharav cyclone - Observations and some theoretical considerations, *J. Geophys. Res., 94*, 18,495-18,514, 1989.

Alpert, P., Y. Shay-El, Y.J. Kaufman, D. Tanre, A. DaSilva, S. Schubert and J.H. Joseph, Quantification of dust-forced heating of the lower troposphere, *Nature, 395*, 367-370, 1998.

Alpert, P., J. Herman, Y. J. Kaufman and I. Carmona, Response of the climatic temperature to dust forcing, inferred from TOMS aerosol index and the NASA assimilation model, *Atmos. Res.*, em 53, 3-14, 2000.

Dulac F., C. Moulin, C. E. Lambert, F. Guillard, J. Poitou, W. Guelle, C. R. Quetel, X. Schneider and U. Ezat, Quantitative remote sensing of African dust transport to the Mediterranean, edited by S. Guerzoni, and R. Chester, *in The Impact of Desert Dust Across the Mediterranean*, pp. 25-49, Kluwer Acad., Norwell, Mass., 1996.

Ganor, E. Analysis of atmospheric dust in Israel, Ph.D. thesis, Hebrew Univ. of Jerusalem (in Hebrew), Jerusalem, Israel, 1975.

Ganor, E., The composition of clay minerals transported to Israel as indicators of Saharan dust emission. *Atmos. Environ., Ser.A, 25*, 2657-2664, 1991.

Ganor, E. The frequency of Saharan dust episodes over Tel-Aviv, Israel. *Atmos. Environ., 28*, 2867-2871, 1994.

Ganor, E. and H.A. Foner, The mineralogical and chemical properties and the behavior of aeolian Saharan dust over Israel, *in The Impact of Desert Dust Across the Mediterranean*, edited by S. Guerzoni and R. Chester, pp. 163-172, Kluwer Acad., 1996.

Ganor, E., H. Foner, S. Brenner, E. Ne'eman and N. Lavi, The characteristics of settling particles following Saharan dust storms in Israel, *Atmos. Environ., Ser. A., 25*, 2665-2670, 1991.

Guerzoni, S. and R. Chester, *The Impact of Desert Dust Across the Mediterranean*, 389 pp., Kluwer Acad., 1996.

Herman, J. R., P.K. Bhartia, O. Torres, C. Hsu, C. Seftor, and E. Celarier, Global distribution of UV - absorbing aerosols from Nimbus - 7 TOMS data, *J. Geophys. Res., 102*, 16,911-16,922, 1997.

Hsu, N. C., J. R. Herman, O. Torres, B. N. Holben, D. Tanre, T. F. Eck, A. Smirnov, B. Chatenet and F. Lavenu, Comparisons of TOMS aerosol index with sun-photometer aerosol optical thickness: Results and applications, *J. Geophys. Res., 104*, 6269-6279, 1999.

Husar R. B., J. M. Prospero, and L. L. Stowe, Characterization of tropospheric aerosols over the oceans with the NOAA advanced very high resolution radiometer optical thickness operational product, *J. Geophys. Res., 102*, 16,889-16,910, 1997.

Intergovermental Panel on Climate Change, (IPCC), *Climate Change* 1995, *Impacts, Adaptations and Mitigation of Climate Change: Scientific−technical Analyses.* Intergovernmental Panel on Climate Change. Edited by, R. T. Watson, N. C. Zinyowera, R.H. Moss and D.J. Dokken, Cambridge Univ. Press, New York, 1996.

Jankoviak, I. and D. Tanre, Satellite climatology of Saharan dust outbreaks: Method and preliminary results, *J. Clim., 15*, 646-656, 1992.

Levin, Z. E. Ganor and V. Gladstein, The effects of desert particle coated with sulphate on rain formation in the eastern Mediterranean. *Bull. Am. Meteorol. Soc., 35*, 3881-3889, 1996.

Moulin, C., C. E., Lambert, F., Dulac and U., Dayan, Control of atmospheric export of dust from north Africa by the North Atlantic oscillation, *Nature, 387*, 691-694, 1997.

Prospero, J. M. and Nees, R. T. Impact of the North African

drought and El Nino on the mineral dust in the Barbados trade winds, *Nature, 320*, 735-738, 1986.

Pye K., *Aeolian Dusts and Dust Deposits*, Academic, San Diego, Calif., 1987.

Schulz, L. W., J. M. Prospero, and P. Buat-Menard, The long-range transport of mineral aerosols: Gr–oup Report, in *The Long-Range Atmospheric Tra–nsport of Natural and Contaminant Substances.* Kluwer A. H. Knap, edited by Acad., Norwell, Mass., pp. 197-230, 1990.

Tanre, D., Y. J., Kaufman,, M., Herman, and S., Mattoo, Remote sensing of aerosol over oceans using the EOS-MODIS spectral radiances, *J. Geophys. Res., 102*, 16,971-16,988, 1997.

Tegen, I., A. A., Lacis, and I., Fung, The influence of mineral aerosols from disturbed soils on the global radiation budget, *Nature, 380*, 419-422 (1996).

P. Alpert, E. Ganor, Department of Geophysics and Planetary Sciences, Tel Aviv University, Ramat Aviv, Tel Aviv, Israel 69978. (pinhas@cyclone.tau.ac.il)

(Received January 19, 2000; revised June 2, 2000; accepted June 7, 2000.)